Low-cost method to prepare carbon-silica composite mesoporous material from coal gasification fine slag and its application in dye removal

Shuo Liu[1], Jilun Wei[2], Xingtong Chen[1], Weidong Ai[1], Cundi Wei*[1]

[1]Key Laboratory of Automobile Materials of Ministry of Education, College of Materials Science and Engineering, Jilin University, Changchun, 130025, Jilin Prov., China

[2]Department of Chemistry, College of Liberal Art and Science, Arizona State University, Tempe, 85381, Arizona State, The United States

Shuo Liu, Email: liushuo940313@163.com

Jilun Wei, Email: w790896570@outlook.com

Xingtong Chen, Email: chenxt16@mails.jlu.edu.cn

Weidong Ai, Email: 940376948@qq.com

Cundi Wei *, Email: weicundi_jlu@163.com

Tel: +8613514494566

Abstract

The high preparation cost of mesoporous materials limits their practical production and application. This research used the solid waste coal gasification fine slag (FS) as raw material to prepare carbon-silica composite mesoporous material (CSM). Coal gasification fine slag consists of carbon and molten inorganic microspheres. The carbon has a natural mesoporous structure, and the leaching out of metal oxides in the inorganic microspheres generated mesoporous silica, which was confirmed by TEM. Based on the natural properties of coal gasification fine slag, using simple acid leaching technique, carbon-silica composite mesoporous material with specific surface area of 500 m^2/g and pore volume of 0.54 cm^3/g was successfully formed. In addition, the methylene blue adsorption experiment on the prepared CSM showed a maximum adsorption capacity of 182.48 mg/g. This study invented a very economical method to produce mesoporous material.

Key words: Coal gasification slag; Mesoporous carbon; Mesoporous silica; Acid leaching method; Methylene blue

1. Introduction

Due to the energy structure of rich in coal and poor in petroleum and natural gas in China，the coal gasification industry has gained fast development in recent years. According to incomplete statistics[1], around 700 coal gasification furnaces have been put into production. In 2015, more than 250 million tons of coal was consumed and over one hundred million tons of coal gasification slag was produced, and this number has been increasing rapidly. In order to minimize environmental destruction caused by the coal gasification industry, it is necessary to recycle and utilize this solid waste.

Coal gasification slag can be divided into coarse slag (CS) and fine slag (FS). The coarse slag is discharged from the lock hopper and the fine slag is discharged from the filter[2]. Neither is a desirable padding material due to their high carbon content. Many studies have reported the characteristics of carbon in coal gasification slag[3-6]. Wu et al.[4] discovered that the carbon residue in coal gasification slag originates from volatile matters of original coal pyrolysis, partly-gasified carbons, and/or unreacted pyrolytic carbons, and fine slag has a relatively complete porous structure. For the inorganic components, Zhao et al.[7] reported that they existed as molten microspheres in fine slag.

So far, some researches have reported the utilization of coal gasification slag to prepare porous materials. For example, Gu et al.[8] used coal gasification slag as raw material, through KOH activation method at 1037K, formed CSC with specific surface area of 1347 m^2g^{-1} and pore volume of 0.69 cm^3g^{-1}. Li et al.[9] used fine slag as the silica source and through the sol-gel method, prepared MCM-41 with specific surface area of 1347 m^2g^{-1} and pore volume of 0.83 cm^3g^{-1}. However, even though these resultant porous materials have enormous specific surface area and excellent properties, all of them need a high cost of preparation, making it difficult to achieve industrial production. This research solved these problems because no any additives and special reacting conditions were needed.

Mesoporous materials have potential widespread application in adsorption[10-12], catalytic chemistry[13], electrochemistry[14], biosciences[15] and other fields due to their large specific surface area, controllable surface groups and various pore structures. At present, the majority of mesoporous materials are prepared by the template method. The expensive organic additives and complex process of the template method limit its industrial application. Many studies tried to reduce the template method's preparation cost by using inexpensive raw materials or solid wastes[16, 17] but didn't generate ideal effect due to the complicated process.

This study used the simple acid leaching technique to prepare mesoporous material. Li et al.[18] used acid leaching method to prepare mesoporous silica from coal fly ash. However, their method required pretreatment of fly ash and CaO at 1200 °C before the leaching step. This research selected coal gasification fine slag as the raw material. Unlike fly ash, the coal gasification fine slag didn't require a pretreatment step, which significantly reduced the preparation cost. Moreover, the methylene blue adsorption experiment of prepared mesoporous material was conducted. Compared with more than 180 low-cost methylene blue adsorbents provided by Rafatullah et al[19], this carbon-silica composite mesoporous material showed excellent adsorption capacity and attractive price/performance ratio.

2. Experimental Section

2.1 Characterization Methods

The carbon content was measured by a thermo-gravimetric analyzer (model TGA8000) at 700 °C in O_2 atmosphere (Ignoring trace H, S and other elements, the loss on ignition was approximated to be carbon). The ash compositions were determined by the silicate rock chemical analysis method with Chinese standards of GB/T 14506.3-2010 (SiO_2), GB/T 14506.4-2010 (Al_2O_3), GB/T 14506.5-2010 (Fe_2O_3) and GB/T 14506.6-2010 (CaO). The contents of various metal oxides in solution were measured by an

inductively coupled plasma emission spectrometer (model ICP-7400). Metal oxide leaching rate (γ) was calculated according to equation (1):

$$\gamma = (m_2/m_1) \times 100\% \quad (1)$$

where m_1 (g) is the quantity of metal oxide in raw materials; m_2 (g) is the quantity of the leached metal oxide.

The specific surface area and pore structure were characterized by the nitrogen adsorption and desorption method using a JWGB analyzer (model JW-BK222). The BET (Brunauer-Emmett-Teller) method and the BJH (Barrett-Joyner-Halenda) method were used to describe specific surface area and pore size distribution, respectively.

The scanning electronic microscopy coupled with an energy dispersive spectrometry (SEM + EDS, model JSM-IT300) was used to observe the morphologies and the compositions of find slag and carbon-silica composite mesoporous material. The transmission electron microscope (TEM，model JEM-F200) was used to observe the pore structures.

The phase composition of carbon-silica composite mesoporous material was analyzed by an X‐ray diffractometer (model DX-2700). The average size of fine slag was measured by a laser particle size instrument (model JL9200).

The methylene blue concentration was measured by a UV spectrophotometer (model T6) at the wavelength of 665 nm.

2.2 Preparation of Carbon-Silica Composite Mesoporous Material (CSM)

The coal gasification slags (fine slag and coarse slag) were provided by Shenhua Neimeng Coal Industry Group Co., Ltd. Firstly, fine slag was diluted with water until

the solid content was 20 wt%. Then it was hydrocycloned and sieved into FS1~FS5 (The chemical compositions and average particle sizes of FS1~FS5 and coarse slag (CS) are shown in Table1). After drying, 10 g coal gasification slag (fine slag FS1~FS5 and coarse slag) and 50 ml hydrochloric acid (weight concentration between 0 wt% and 20 wt %) were mixed in a flask. The mixture was stirred by a magnetic stirrer at 300 rpm. After 3 hours of stirring at room temperature, the mixture was filtered to obtain solids. The solids were washed with distilled water to remove residual ions in the pores and then dried at 120 °C for 12 h to obtain the mesoporous material CSM.

2.3 Methylene Blue Adsorption Experiment

The methylene blue (MB) was bought from Shenyang Le Heng Technology Co., Ltd, which was used to measure CSM's capability in organic dye removal. The adsorption experiment was performed in a beaker with 0.1 g CSM and 100 ml MB solution (initial concentration varied from 60 to 200 mg/L). The beaker was magnetically stirred for 24 h at different temperatures (298K, 318K, 338K) for the reaction to reach equilibrium. Then, the suspension was centrifuged for 10 min at 15,000 rpm to obtain supernatant solution. The amount of MB absorbed at equilibrium Q_e (mg/g) was calculated by equation (2):

$$Q_e = V(C_0 - C_e)/W \quad (2)$$

where C_0 and C_e (mg/L) are the liquid-phase concentrations of MB in the beginning and at equilibrium. V (L) is the volume of MB solution, and W (g) is the mass of CSM used.

The Freundlich Linear Model[20] (equation 3) and Langmuir Linear Model[21] (equation 4) were used to fit the equilibrium adsorption isotherms of MB.

$$\ln Q_e = \ln k_F + (1/n)\ln C_e \quad (3)$$

$$C_e/Q_e = 1/Q_m k_L + C_e/Q_m \quad (4)$$

where k_F is the Freundlich constant ($(mg\cdot g^{-1})(mg\cdot L^{-1})^{-1/n}$), $1/n$ is the heterogeneity factor; Q_m is the maximum adsorption capacity ($mg\cdot g^{-1}$) and k_L is the Langmuir

constant ($L \cdot mg^{-1}$).

The kinetic testing process was similar to the equilibrium testing. The influence of reaction time on MB adsorption was studied with 100 mg/L MB solution at 298K. The reaction time was varied from 0 to 100 min. The amount of MB absorbed at time t, Q_t (mg/g), was calculated by equation (5):

$$Q_t = V(C_0 - C_t)/W \quad (5)$$

where C_0 and C_t (mg/L) are the liquid-phase concentrations of MB in the beginning and at time t. V (L) is the volume of MB solution, and W (g) is the mass of CSM used.

The Pseudo-First-Order Kinetic Model[22] (equation 6) and Pseudo-Second-Order Kinetic Model[23] (equation 7) were used to fit the kinetic parameters of the adsorption process .

$$\ln(Q_e - Q_t) = \ln Q_e - (k_1/2.303)t \quad (6)$$

$$t/Q_t = 1/k_2 Q_e^2 + (1/Q_e)t \quad (7)$$

where k_1 is the first-order adsorption rate constant, and k_2 is the second-order adsorption rate constant.

3. Results and Discussion

3.1 Influencing factors on CSM's Pore Structure

Based on the natural pore structure of the unburned carbon in the coal gasification fine slag, the carbon-silica composite mesoporous material (CSM) was prepared by leaching out metal oxides resided in the inorganic molten microspheres. The properties of coal gasification fine slag and reaction conditions such as hydrochloric acid dosage, reaction time and reaction temperature may affect resultant CSM's specific surface area and pore structure. Experimental results showed that the impacts of reaction time and reaction temperature were very small (*See Table S1 and Table S2 in Supporting Information*), and the main influencing factors on CMS's pore structure were acid concentration and particle size of coal gasification slag, which will be discussed separately in the following sections.

3.1.1 Influence of acid concentration on CSM's pore structure

Sample FS3 was selected as the raw material to study the relationship among acid concentration, leaching conditions and CSM's pore structure. Figure 1 shows the influence of acid concentration on metal oxides' leaching rate. *(Detailed information about the leaching mass and leaching rate of all metal oxides under different acid concentrations are shown in Table S3 in Supporting Information.)* With the increase of hydrochloric acid concentration, the leaching rates were increased. Under the same acid concentration, the leaching rates of all metal oxides were similar (except CaO whose bond breaking contributed to slightly higher leaching rate at low acid concentrations). This indicated that almost all metal oxides were leached out at the same time during the reaction. At the acid concentration of 16 wt%, the total leaching rate got the maximum value of 82%, with Al_2O_3 being 82%, CaO being 91%, Fe_2O_3 being 89% and others being 70%.

Figure 2 shows the influence of acid concentration on CSM's specific surface area and pore volume. (*Detailed information can be found in Table S4 in Supporting Information.*) The specific surface area and pore volume of the raw material (sample FS3, at 0 wt% acid concentration) were 121 m^2/g and 0.126 cm^3/g, respectively. When FS3 were reacting with the hydrochloric acid, the metal oxides in the inorganic microspheres were leached out and a porous silica structure was formed. As the acid concentration was increased, more and more metal oxides were leached out and the porous silica structure's specific surface area and pore volume were increased accordingly. At 16 wt% acid concentration, the highest specific surface area and pore volume were obtained. Combining results in Figure 1, the optimum acid concentration for the leaching reaction was 16 wt%.

Figure 3 shows the pore size distribution of raw material FS3 and resultant CSMs formed with different acid concentrations. Before leaching, all of the pores in the raw

material existed in the carbon area, the size of which were between 2~5 nm. After leaching, the number of pores with sizes between 2~5 nm increased significantly, while the number of pores outside this range almost didn't change, regardless of acid concentration used for the leaching. This suggested that the size of metal oxides in the inorganic microspheres were around 2~5 nm. Removal of metal oxides contributed to more pores with sizes between 2~5 nm. Therefore, in CSM, the carbon and silica have a similar pore size distribution of 2~5 nm.

3.1.2 Influence of fine slag's particle size on CSM's pore structure

The particle size of coal gasification slag is another important influencing factor on CSM's pore structure. It has a significant impact on the pore structure of both carbon and silica in CSM. Table 2 shows the pore properties of several coal gasification slags (fine slags FS1~FS5 and coarse slag). The small specific surface area and pore volume suggested that the coarse slag didn't have a porous structure. What's more, the inorganic component of coarse slag is in the form of block with a large particle size. Therefore, coarse slag was not a desirable raw material for the preparation of mesoporous materials. As for fine slag, in the process of coal gasification, the unburned carbon is activated by water vapor, carbon dioxide and other gases at high temperature to form activated carbon with high surface area. According to table 1 and table 2, fine slags with smaller particle size showed higher specific surface area and pore volume. This was probably because during the gasification process, the small carbon particles had relatively larger contact area with the surrounding gases, contributing to the further dredging of pore channels.

Figure 4 shows the leaching rate of metal oxides in different fine slags (FS1~FS5) at the optimal acid concentration of 16 wt%. (*The detailed leaching mass and leaching rate of FS1~FS5 is shown in Table S5 in Supporting Information.)* The fine slags with smaller particle size showed higher leaching rate than those with larger particle size. Figure 5

shows the specific surface area and pore volume of CSM1~CSM5 prepared from FS1~FS5, respectively. (*The specific data is shown in Table S6 in Supporting Information.)* It can be seen in the figure that fine slags with smaller particle size led to the formation of CSM with higher specific surface area and pore volume. Therefore, the richer pore structure in natural carbon component and higher leaching rate of metal oxides from inorganic microspheres contributed to the formation of the more abundant porous structure of finer slags.

The optimal carbon-silica composite mesoporous material produced in the current work was CSM1 prepared from the finest coal gasification slag FS1, which showed the highest specific surface area (500 m^2/g) and pore volume (0.54 cm^3/g). It was selected as the CSM sample for the subsequent characterizations. Table 3 shows the chemical composition of CSM1. Due to the limitation of the acid leaching technique, some metal oxides impurities were present. The XRD diffraction image of CSM1 is shown in Figure 6. The image indicated that CSM1 had an amorphous structure. This was because the particle size of FS1 was very small, causing its relative large heat-receiving area during the gasification process, and leading its inorganic components to completely melt. Figure 7 (a) shows the pore size distribution of CSM1. From the figure we can see that CSM1 was a mesoporous material with pore sizes distributed widely within the 2~50 nm range. However, majority of the pores were about 2~5 nm large. Figure 7 (b) shows the N_2-adsorption/desorption isotherms of CSM1. However, since the inorganic substances were in the molten state, removal of the metal oxides led to the formation of pores with irregular shapes. Therefore, the adsorption/desorption isotherms normally used to characterize pores of regular shapes were not applicable here.

3.2 Morphology characterization

Figure 8 shows the scanning electronic microscopy coupled with energy dispersive spectrometry (SEM & EDS) patterns of the raw material FS1 (a, c) and the product

CSM1 (b, d). It can be seen in figure 8 (a) that FS1 consisted of flocculated unburned carbon component and molten spherical inorganic components, the morphology of which was similar to the morphology reported by Wu et al[24] for coal gasification fine slag. The spherical structure of inorganic substances is due to the complete melting of small particle minerals at high temperature during coal gasification. Then, the liquid cooled rapidly into amorphous microspheres under the action of surface tension. The microspheres in FS1 varied significantly in size. The diameter of the large spheres was in micro-scale, while the diameter of the small spheres was in nano-scale. The morphology of CSM1 produced in this work was similar to the morphology of the raw material FS1, but the amount of metal elements in the inorganic spheres of CMS1 was much less than that of FS1, as is shown by the EDS patterns (c, d). This indicated that a significant amount of metal oxides were leached out from CSM1 during the reaction with hydrochloric acid. Due to the limitation of SEM's magnification, the pore structure could not be observed, and TEM was used instead. The TEM images of FS1 (a) and CSM1 (b) are shown in Figure 9. It can be clearly seen that the carbon component showed porous structure both in FS1 and CSM1. However, the inorganic microspheres only showed a porous structure in CSM1. The inorganic microspheres in FS1 showed very smooth surface, which was indication of a solid structure. The TEM images confirmed the formation of mesoporous silica in coal gasification fine slag by the acid leaching technique.

3.3 The application of CSM in dye removal

Wastewater discharged from textile, printing & dyeing, paper, cosmetics and other industries contains a large amount of organic dyes, which are toxic to aquatic organisms. Methylene blue (MB, $C_{16}H_{18}ClN_3S$), a widely used organic cationic dye, was used as the testing agent of dye removal effect in most studies. Figure 10 shows the impact of contact time on methylene blue adsorption onto CSM1 at 298K. The adsorption was very rapid in the beginning. Then，as more and more sorption sites became saturated and

the concentration of methylene blue was decreased, the adsorption driving force (concentration gradient) was reduced, leading to the slowdown of the adsorption rate and eventually nearly stop.

To study the kinetic aspects of the adsorption process, experimental data was fitted to the Pseudo-First-Order kinetic model and Pseudo-Second-Order kinetic model. The fitting parameters are presented in Table 4, and the linear regression equations are shown in Figure 11. The linear relationship of t/q_t versus t in the Pseudo-Second-Order model showed good agreement between experimental and calculated values. Moreover, the correlation coefficients (R) of the second-order kinetic model was greater than 0.99, and the calculated Q_e of the second-order kinetic model was very close to experimental value. Therefore, MB adsorption onto CSM1 conducted according to the pseudo-second-order kinetic model. This indicated that during the adsorption, there was electron sharing and electron transfer between the adsorbate and adsorbent, which was characteristic of chemical adsorption.

The equilibrium sorption isotherms of MB onto CSM1 with initial MB concentration of 60~200 mg/L at 298K, 318K and 338K are shown in Figure 12. The equilibrium sorption amount increased with the increase of initial MB concentration. At low MB concentrations, there were not enough MB molecules to occupy all the sorption sites. Thus, the higher the MB concentration, i.e. the more MB molecules surrounding the active sorption sites, the higher the equilibrium sorption amount (Q_e). At high MB concentrations, the increase in equilibrium sorption amount was slowed down. This was because most of the sorption sites were occupied by MB molecules, and the number of vacant sites available for sorption became limited. Thus, further increase in MB concentration wouldn’t contribute much to the adsorption of more MB molecules. In addition, Figure 12 shows that the equilibrium sorption amount decreased with the increase of temperature. This phenomenon indicated that the adsorption of MB onto

MCS was an exothermic process.

The equilibrium adsorption isotherm is also used to describe the distribution of the adsorbate molecules between the liquid and the solid phases at equilibrium state. The experimental sorption data was fitted to the widely used Freundlich and Langmuir models. The fitting to the linear regression equations are shown in Figure 13 and fitting parameters are shown in Table 5. By comparison, the Langmuir model showed a better fitting at all temperatures. The linear correlation coefficients of the Langmuir model at 298K, 318K and 338K were all over 0.99, indicating high applicability between the experimental data and Langmuir isotherms. This indicated that the CSM1 surface was covered by a monolayer of uniformly distributed MB molecules.

According to Table 5, the maximum adsorption capacity of methylene blue onto CSM1 can reach up to 182.48 mg/g. This may because H^+ combined with surface "Si-O-" defects of silica to form silanol groups during acid treatment process. Hydrogen bonds and/or electrostatic interactions formed between methylene blue and silanol groups, increasing the adsorption capacity. Table 6 shows the maximum adsorption capacity of several activated carbons and porous silica made from different solid wastes as well as the preparation methods. By comparison, no need for any additive, high temperature and special atmosphere conditions, CSM1 has the lowest preparation cost, which can completely achieve large-scale industrial production. However, its adsorption capacity surpassed majority of the porous materials listed in the table. In an review article written by Rafatullah et al.[19], more than 180 low-cost adsorbents for methylene blue adsorption were presented, which included various commercial activated carbons, biomass activated carbons, natural materials, bioadsorbents, zeolites and other siliceous materials. Compared with those materials, CSM1 still displayed an extremely high price/performance ratio. With low production cost and excellent adsorption capability, the coal gasification slag-based carbon-silica composite mesoporous material has great

potential in the application of industrial wastewater dye removal.

4. Conclusion

In this research, the low-cost acid leaching method was used to prepare carbon-silica composite mesoporous material from coal gasification fine slag. This method overcame the difficulties of industrialized processes for the preparation of mesoporous materials, which enabled its application in general fields. Coal gasification fine slag consists of natural mesoporous carbon component and molten inorganic microspheres, and the mesoporous carbon-silica composite material was formed by leaching out metal oxides resided in the inorganic microspheres. The optimal acid concentration for the leaching reaction was 16 wt%, and fine slags with smaller particle size resulted in the formation of CSMs with higher specific surface area, larger pore volume and better adsorption capability. The best carbon-silica composite mesoporous material prepared in this work, CSM1, showed specific surface area of 500 m^2/g, pore volume of 0.54 cm^3/g, and pore size mainly distributed between 2 and 5 nm. The methylene blue adsorption experiments suggested that sorption onto CSM1 followed the Pseudo-Second-Order kinetic model and the Langmuir equilibrium model. The maximum adsorption capacity of CSM1 was 182.48 mg/g, indicating its great potential in the application of dye removal.

Acknowledgment

This study is financially supported by Jilin Province/ Jilin University Co-construction Project – Funds for New Materials (SXGJSF2017-3).

References

1. S. Wang, *CHEMICAL INDUSTRY AND ENGINEERING PROGRESS*, 2016, 35, 653-664.
2. C. Pan, Q. Liang, X. Guo, Z. Dai, H. Liu and X. Gong, *Energy & Fuels*, 2016, 30, 1487-1495.
3. N. J. Wagner, R. H. Matjie, J. H. Slaghuis and J. H. P. van Heerden, *Fuel*, 2008, 87, 683-691.
4. S. Wu, S. Huang, L. Ji, Y. Wu and J. Gao, *Fuel*, 2014, 122, 67-75.
5. T. Wu, M. Gong, E. Lester, F. Wang, Z. Zhou and Z. Yu, *Fuel*, 2007, 86, 972-982.
6. S. Xu, Z. Zhou, X. Gao, G. Yu and X. Gong, *Fuel Processing Technology*, 2009, 90, 1062-1070.
7. X. Zhao, C. Zeng, Y. Mao, W. Li, Y. Peng, T. Wang, B. Eiteneer, V. Zamansky and T. Fletcher, *Energy & Fuels*, 2010, 24, 91-94.
8. Y.-y. Gu and X.-c. Qiao, *Microporous and Mesoporous Materials*, 2018, DOI: 10.1016/j.micromeso.2018.06.025.
9. C.-c. Li, X.-c. Qiao and J.-g. Yu, *Materials Letters*, 2016, 167, 246-249.
10. C.-X. Gui, Q.-J. Li, L.-L. Lv, J. Qu, Q.-Q. Wang, S.-M. Hao and Z.-Z. Yu, *Rsc Advances*, 2015, 5, 20440-20445.
11. F. Gu, M. Liang, D. Han and Z. Wang, *Rsc Advances*, 2015, 5, 39964-39972.
12. S. Zeng, R. Wang, Z. Zhang and S. Qiu, *Rsc Advances*, 2016, 6, 49551-49555.
13. Z.-M. Cui, J. Hao, J. Liu and W.-G. Song, *Rsc Advances*, 2016, 6, 74545-74549.
14. L. Liu, C. Tong, Y. He, Y. Zhao, B. Hu and C. Lu, *Rsc Advances*, 2015, 5, 43381-43390.
15. M. M. Ayad, N. A. Salahuddin, N. L. Torad and A. Abu El-Nasr, *Rsc Advances*, 2016, 6, 57929-57940.
16. X. Castillo, J. Pizarro, C. Ortiz, H. Cid, M. Flores, E. De Canck and P. Van Der Voort, *Microporous and Mesoporous Materials*, 2018, 272, 184-192.
17. F. Yan, J. Jiang, S. Tian, Z. Liu, J. Shi, K. Li, X. Chen and Y. Xu, *Acs Sustainable Chemistry & Engineering*, 2016, 4, 4654-4661.
18. C.-c. Li and X.-c. Qiao, *Chemical Engineering Journal*, 2016, 302, 388-394.
19. M. Rafatullah, O. Sulaiman, R. Hashim and A. Ahmad, *Journal Of Hazardous Materials*, 2010, 177, 70-80.
20. H. Freundlich, *Transactions of the Faraday Society*, 1932, 38, 0195-0201.
21. I. Langmuir, *Journal of the American Chemical Society*, 1916, 38, 2221-2295.
22. S. Lagergren and B. K. Svenska, *The Royal Swedish Academy of Sciences Document*, 1898, 24, 1-13.
23. Y. S. Ho and G. McKay, *Process Biochemistry*, 1999, 34, 451-465.
24. S. Wu, S. Huang, Y. Wu and J. Gao, *Journal Of the Energy Institute*, 2015, 88, 93-103.
25. M. A. Islam, M. J. Ahmed, W. A. Khanday, M. Asif and B. H. Hameed, *Ecotoxicology And Environmental Safety*, 2017, 138, 279-285.
26. C. Zhou, Q. Gao, W. Luo, Q. Zhou, H. Wang, C. Yan and P. Duan, *Journal Of the Taiwan Institute Of Chemical Engineers*, 2015, 52, 147-157.
27. M. A. Franciski, E. C. Peres, M. Godinho, D. Perondi, E. L. Foletto, G. C. Collazzo and

G. L. Dotto, *Waste Management*, 2018, 78, 630-638.
28. G. Yang, Y. Deng and J. Wang, *Ceramics International*, 2014, 40, 7401-7406.
29. J.-M. Hong, B. Lin, J.-S. Jiang, B.-Y. Chen and C.-T. Chang, *Journal Of Industrial And Engineering Chemistry*, 2014, 20, 3667-3671.
30. M. Salmi, S. Balou, K. Kohansal, K. Babaei, A. Tavasoli and M. Andache, *Energy & Fuels*, 2017, 31, 12327-12338.
31. C. Wang, J. Li, L. Wang, X. Sun and J. Huang, *Chinese Journal Of Chemical Engineering*, 2009, 17, 513-521.
32. R. M. Novais, G. Ascensao, D. M. Tobaldi, M. P. Seabra and J. A. Labrincha, *Journal Of Cleaner Production*, 2018, 171, 783-794.
33. Y. C. Sharma, Uma and S. N. Upadhyay, *Energy & Fuels*, 2009, 23, 2983-2988.

Tables

Table 1 Chemical compositions (wt %) and average particle sizes of FS1~FS5 and CS

Sample	D_{av}	SiO2	Al2O3	Fe2O3	CaO	Others	Carbon
FS1	6.1	41.54	15.98	5.21	10.95	8.93	17.39
FS2	7.3	40.02	15.86	5.89	10.14	8.11	19.72
FS3	10.0	38.78	17.31	5.75	7.38	7.60	23.18
FS4	14.6	36.41	16.02	5.38	7.12	6.37	28.70
FS5	22.4	34.21	14.45	4.59	6.95	6.68	33.12
CS	>1000	32.74	14.00	8.52	33.19	4.39	7.18

* D_{av} (μm) is the average particle size.

Table 2 Pore properties of coal gasification fine slags (FS1~FS5) and coarse slag (CS)

Raw material	BET area (m^2/g)	Pore volume (cm^3/g)	Average pore size (nm)
FS1	171	0.161	4.908
FS2	154	0.144	4.792
FS3	121	0.126	5.207
FS4	80	0.064	4.484
FS5	76	0.053	5.687
CS	2	0.003	5.757

Table 3 Chemical composition (wt %) of CSM1

Carbon	SiO_2	Al_2O_3	CaO	Fe_2O_3	Others
27.84	63.82	3.77	0.85	1.09	2.63

Table 4 Adsorption kinetic parameters of methylene blue onto CSM1

First-order	$Q_{e,\,exp}$ (mg/g)	$Q_{e,\,cal}$ (mg/g)	k_1 (min^{-1})	R^2
model	99.20	9.65	0.0625	0.7520
Second-order	$Q_{e,\,exp}$ (mg/g)	$Q_{e,\,cal}$ (mg/g)	k_2 (g/mg·min)	R^2
model	99.20	99.21	0.0102	0.9999

* $Q_{e,\,exp}$ is the experimental data; $Q_{e,\,cal}$ is the calculated data.

Table 5 Fredndlich and Langmuir model parameters of MB adsorption onto CSM1 at different temperatures

Adsorption model	Parameters	Temperature (K)		
		298	318	338
Freundlich	n	4.171	4.188	3.531
	k_F	91.27	86.51	69.69
	R^2	0.9409	0.9665	0.9587
Langmuir	Q_m (mg/g)	182.48	178.25	171.53
	k_L (L/mg)	0.9682	0.8711	0.5123
	R^2	0.9962	0.9956	0.9955

Table 6 Maximum adsorption capacities of several materials prepared from solid wastes

Sample	Raw material	Preparation Method	Q_m (mg/g)	Reference
Activated carbon	Rattan waste	Hydrothermal (200 °C) and NaOH activation (600 °C)	359	[25]
Al-MCM-41	Coal fly ash	Template (ethyl acetate, 550 °C)	278	[26]
Activated carbon	Barley malt bagasse	N_2 pyrolysis (800 °C) and CO_2 activation (900 °C)	161	[27]
MCM-41	Iron ore tailing	Template (CTAB, 550 °C)	111	[28]
Q-MCM	Waste quartz sand	Template (CTAB,550 °C)	97	[29]
Activated carbon	Canola Stalk	KOH activation (700 °C)	93	[30]
Zeolite	Coal fly ash	Hydrothermal (NaOH, 100 °C)	44	[31]
Porous geopolymer	biomass fly ash	sodium silicate, NaOH, H_2O_2	21	[32]
Activated carbon	Coconut coir	$Zncl_2$ activation (700°C)	16	[33]
CSM1	Coal gasification slag	Acid leaching (HCl, room temperature)	182	This research

Figures

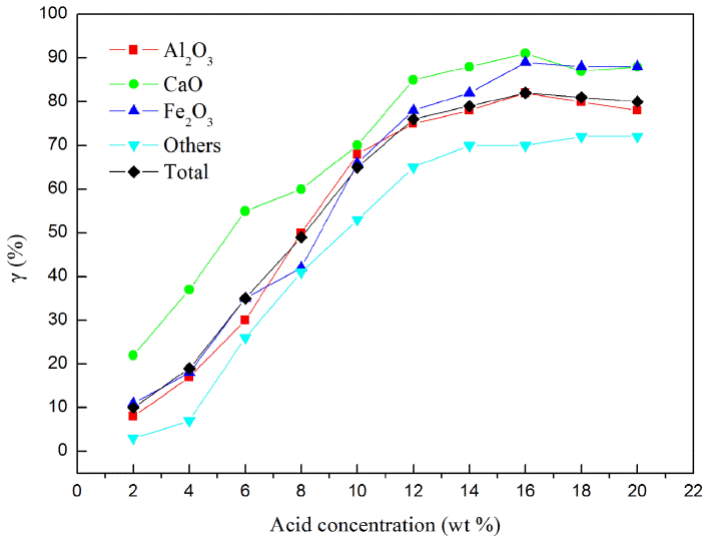

Fig.1 Leaching rate of various metal oxides under different acid concentrations.

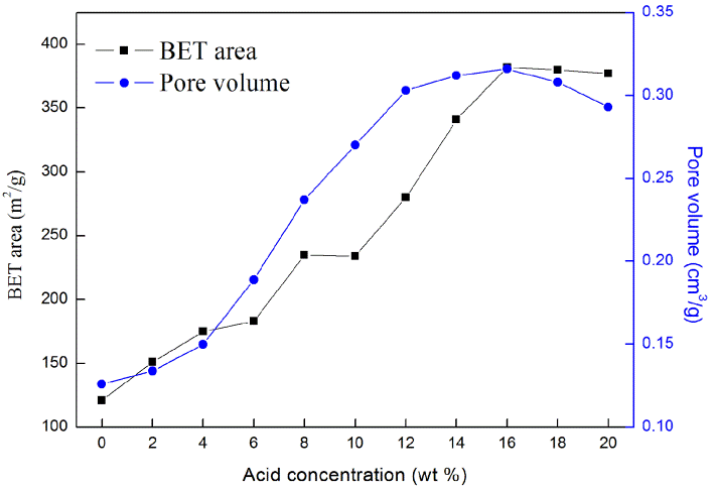

Fig.2 BET specific surface area and pore volume of CSM under different acid concentrations.

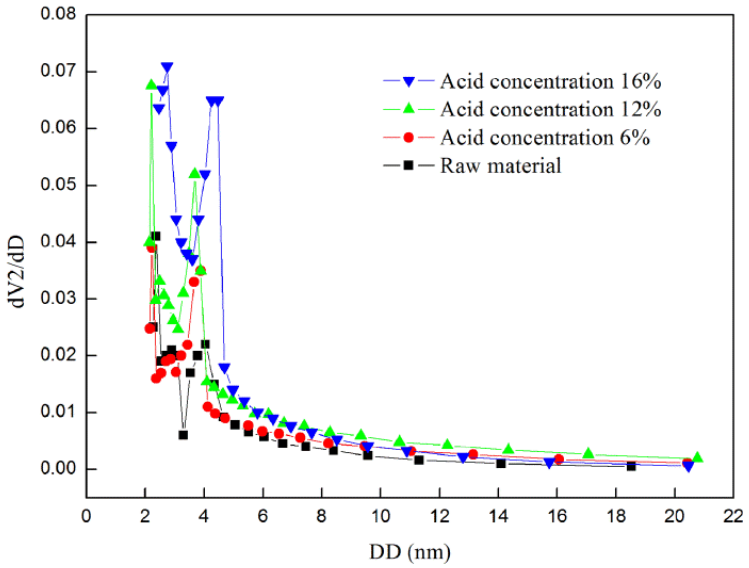

Fig.3 BJH desorption pore size distribution of raw material FS3 and resultant CSMs at acid concentration of 6 wt%, 12 wt% and 16 wt%, respectively.

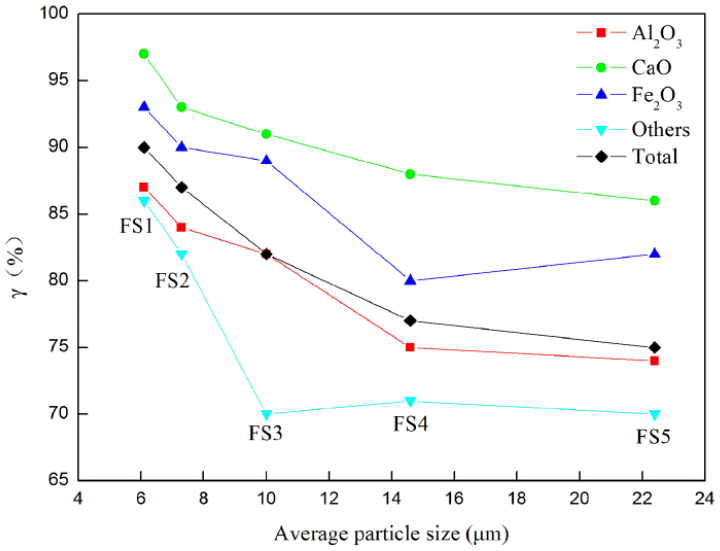

Fig.4 Leaching rate of metal oxides in different fine slags (FS1~FS5) at the optimum acid concentration of 16 wt%.

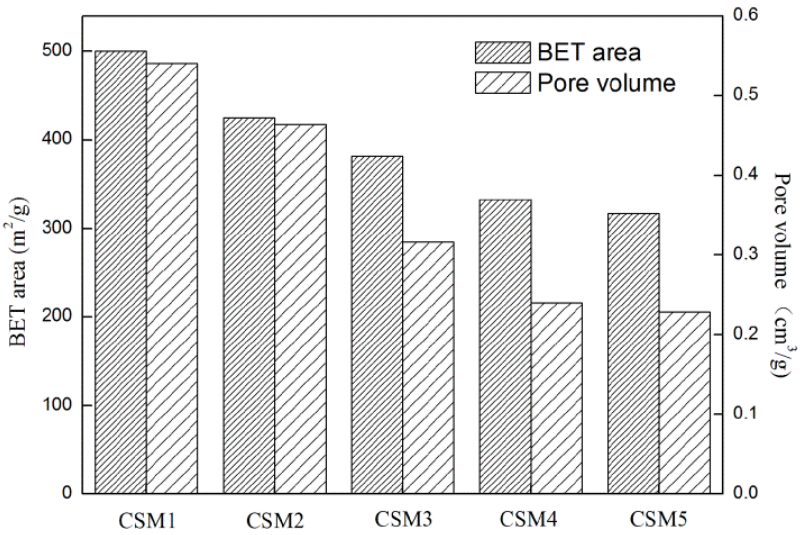

Fig.5 BET area and pore volume of CSM1~CSM5. The CSM1~CSM5 were prepared from raw materials FS1~FS5, respectively.

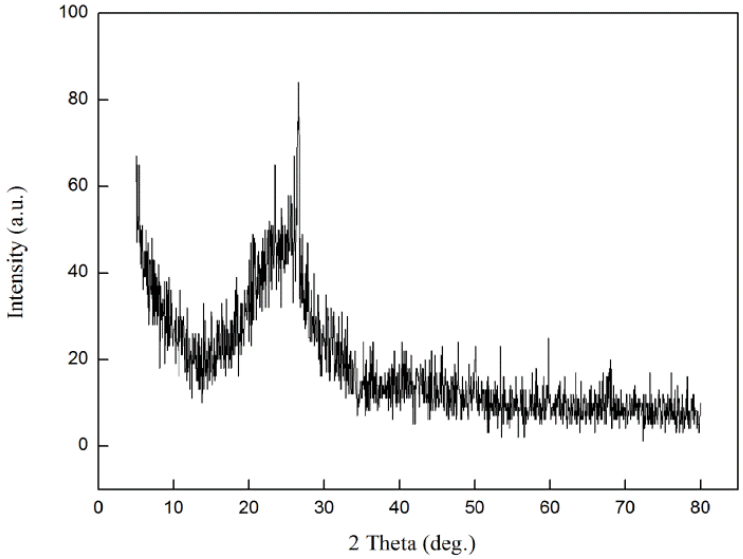

Fig.6 XRD spectrum of CSM1.

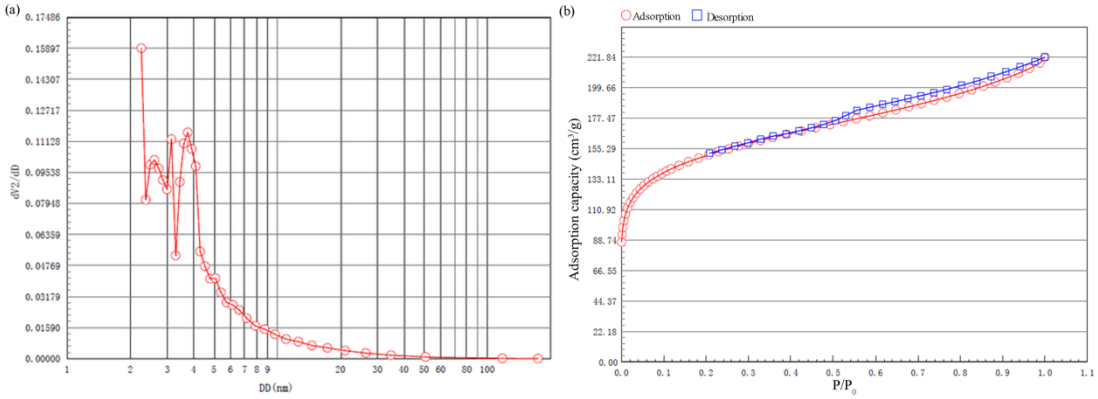

Fig.7 Pore size distribution (a) and N_2-adsorption/desorption isotherms (b) of CSM1.

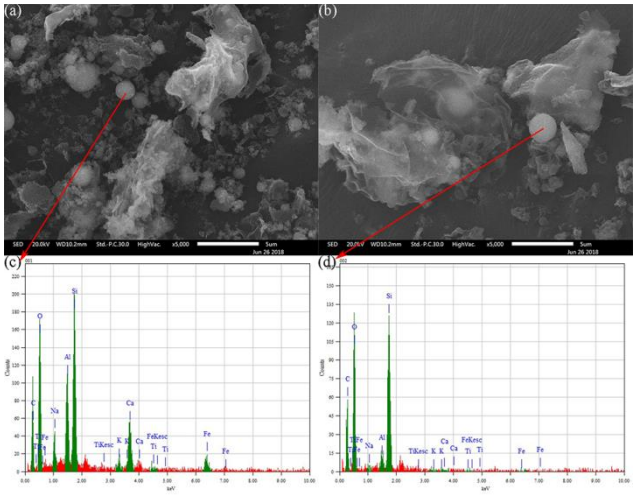

Fig.8 SEM & EDS patterns of FS1 (a, c) and CSM1 (b, d).

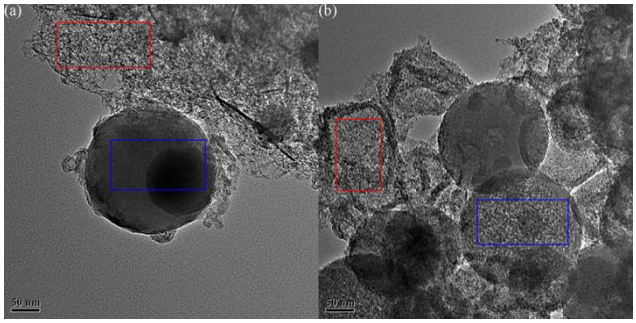

Fig.9 TEM images of raw material FS1 (a) and product CSM1 (b). The red fields show the morphology of carbon and the blue fields show the morphology of silica.

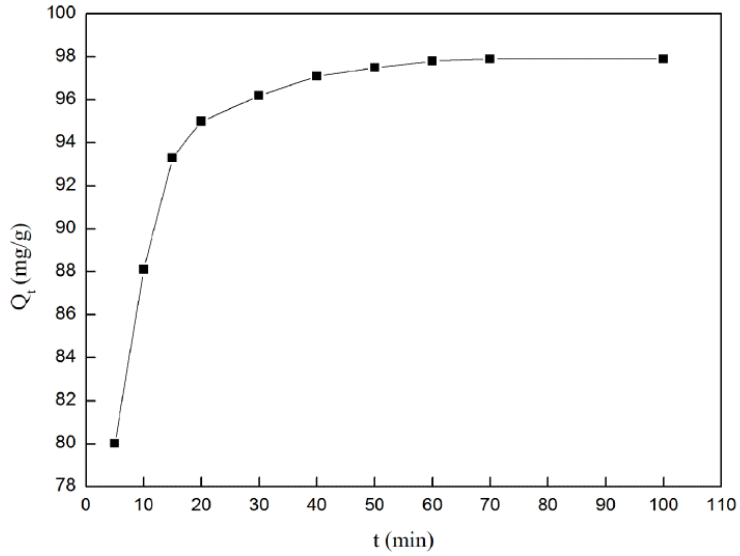

Fig.10 Impact of contact time on the adsorption of methylene blue (MB) onto CSM1 at 298K. The initial concentration of MB was 100 mg/L.

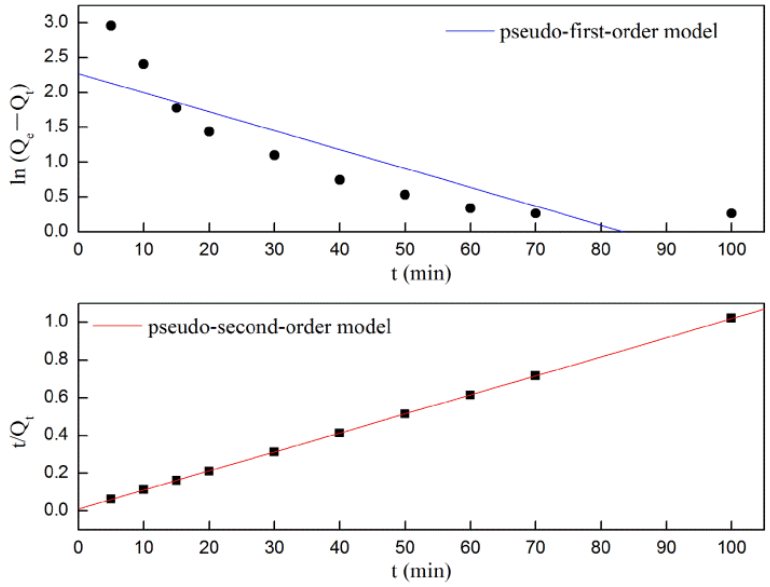

Fig.11 Fitting of kinetic models to CSM1 methylene blue adsorption experimental data.

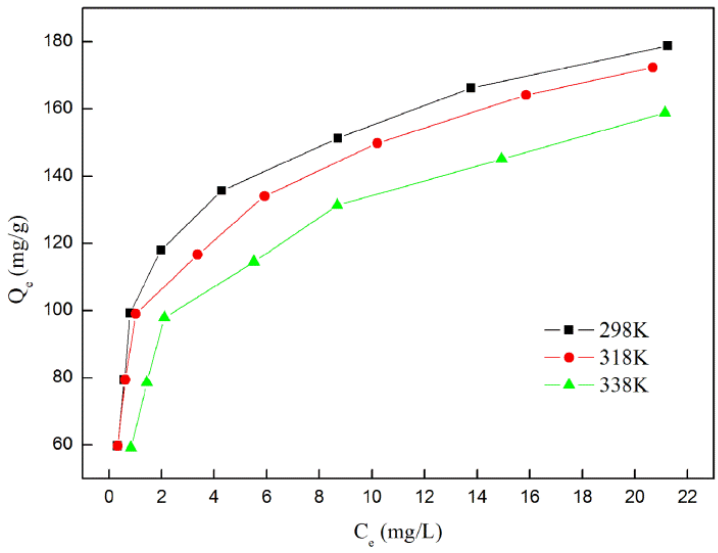

Fig.12 Equilibrium soprtion isotherms of methylene blue onto CSM1 at 298K, 318K and 338K.

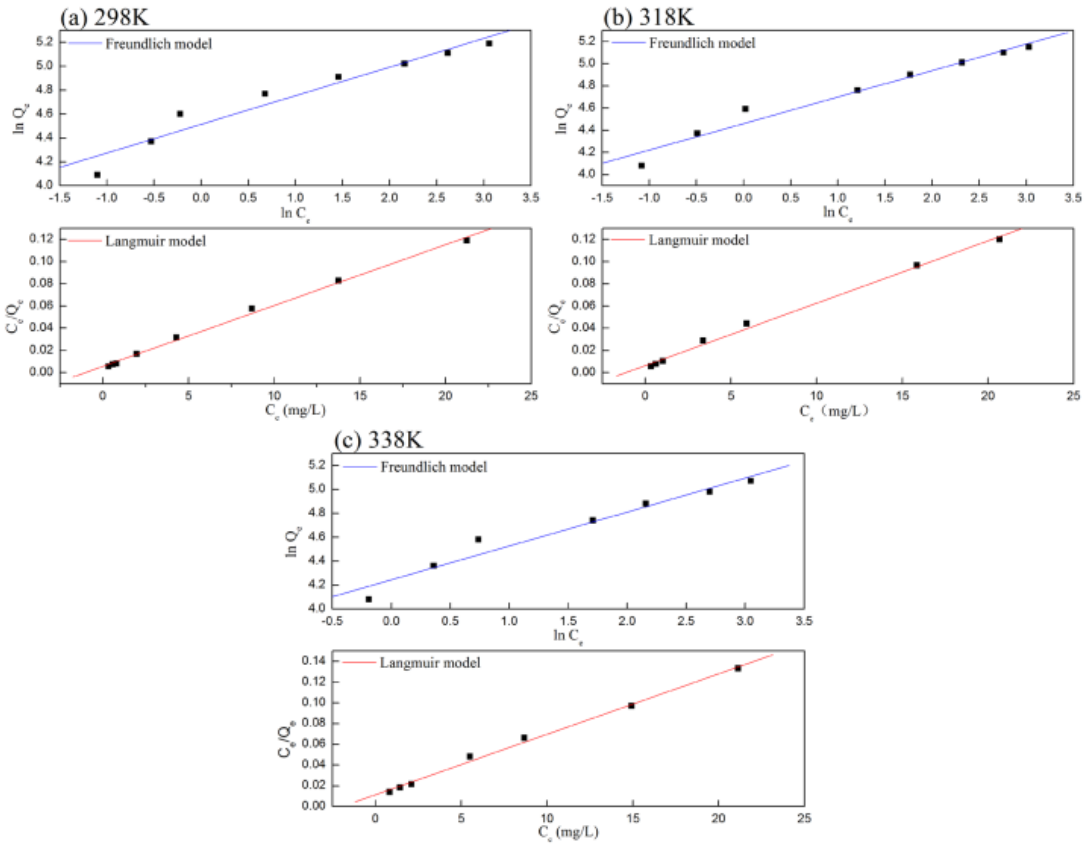

Figu.13 Fitting of Freundlich and Langmuir models to MB adsorption onto CSM1 experimental data at 298K (a), 318K (b) and 338K (c).